JOURNAL OF MATERIALS SCIENCE 37 (2002) 997–1003

Early-stage sintering mechanisms of Fe-doped CeO_2

ZHANG TIANSHU, PETER HING, HAITAO HUANG
Advanced Materials Research Centre, School of Materials Engineering, Nanyang Technological University, Nanyang Avenue, Singapore 639798
E-mail: p142713729@ntu.edu.sg

J. KILNER
Department of Materials, Imperial College of Science, Technology and Medicine, London SW7, 2AZ, UK

Cerium oxide is a very useful base material used as catalyst supports, ion conductors and gas sensors. It is also well known that ceria-based materials are difficult to densify below 1500°C. However, a small amount of Fe doping obviously promotes the densification rate and reduces the sintering temperatures. In this study, the early stage sintering mechanisms of undoped and Fe-doped CeO_2 were investigated, based on two sintering models. We confirm that pure CeO_2 exhibits volume-diffusion controlled sintering, while a viscous flow mechanism dominates the early stage sintering of Fe-doped CeO_2.
© *2002 Kluwer Academic Publishers*

1. Introduction

Two major advantages, high efficiency and very low emission of pollutants, of solid oxide fuel cell (SOFC) systems are very attractive. At the present stage, solid oxide electrolytes for fuel cells are mainly based on yttria stabilized zirconia (YSZ) because of its nearly pure oxygen ionic conductivity in oxidizing or reducing atmosphere and good mechanical properties. In order to maintain high oxygen ionic conductivity, however, high operating temperatures of over 900°C are required for this kind of electrolyte [1–3]. Such high operating temperatures increase fabrication cost and accelerate the degradation of the fuel cell system.

Recently, an intensive investigation is being carried out to reduce the operating temperature of the fuel cell to 500–800°C. Ceria-based materials have been extensively studied because of their high oxygen ionic conductivity at lower temperatures [4–6]. However, CeO_2 based materials are usually difficult to densify below 1500°C [7, 8]. In order to understand the sintering behavior, it is urgent to do same research on the sintering mechanisms. For CeO_2-based materials, some experiments have been conducted on sintering mechanisms. However, most of literature reports concerning sintering study of CeO_2 based-materials concentrate on the final stage sintering. To our knowledge, only few papers dealt with the early-stage sintering of CeO_2-based materials. For example, Zhou and Rahaman [9] studied the early-stage sintering using CeO_2 powders prepared by hydrothermal synthesis. In their paper, a power law $m = 0.5$ was obtained, which is far smaller than the values given by classic models. They gave a very vague and unsatisfactory explanation of this discrepancy.

In our case [10], we found that a small amount of Fe doping (<1% in atomic rato) promotes densification of CeO_2 powder and reduces sintering temperatures by more than 200°C. Moreover, the grain size keeps almost unchanged until relative density reaches over 85%. It suggests that the early-stage sintering may play a very important role in the densification of Fe-doped CeO_2 powder. The sintering process is traditionally classified into three stages, i.e., the initial, intermediate and final stages of sintering [11]. For convenience, the sintering process in this work is divided into two stages, i.e., the early-stage (≤90% of relative density) and final-stage (>90% of relative density) sintering. This is similar to the sintering stages defined by Du and Cocks [12]. In this study, we will concentrate on the early-stage sintering mechanisms of undoped and Fe-doped CeO_2 powders, based on two sintering models. A serial study on the final-stage sintering behavior of Fe-doped CeO_2 ceramics will be reported in our another communication.

2. Data analysis

2.1. Model 1

Bannister [13] suggested a general equation for isothermal initial-stage sintering as follows:

$$\frac{\mathrm{d}}{\mathrm{d}t}(\Delta L/L_0) = A_0 \exp\left(-\frac{Q}{RT}\right) \Big/ (\Delta L/L_0)^m \quad (1)$$

where $\Delta L/L_0$ is relative shrinkage, t is time. A_0 is a constant depending only on the material parameters and the sintering mechanisms. The exponent, m, has values

of $m = 0$ for viscous flow, $m = 1$ for volume diffusion and $m = 2$ for grain boundary diffusion mechanisms. Based on Equation 1, Young and Culter [14] developed the following equation under a constant heating rate condition:

$$(\Delta L/L_0)/T = A_1 \exp\left[-\frac{Q}{(m+1)RT}\right] \quad (2)$$

The natural logarithmic form of Equation 2:

$$\ln[(\Delta L/L_0)/T] = -\frac{Q}{(m+1)R}\frac{1}{T} + \ln A_1 \quad (3)$$

If we can determine the value m, the apparent activation energy, Q, can be calculated from the slope of plot $\ln[(\Delta L/L_0)/T]$ versus $1/T$. Alternatively, the value m can be obtained using either isothermal or nonisothermal techniques. By integrating Equation 1 the following formula can be obtained:

$$(\Delta L/L_0)^{m+1} = A_2 \exp\left(-\frac{Q}{RT}\right)t \quad (4)$$

Equation 4 is the so-called isothermal equation. The value m can be obtained from the natural logarithm of $[(\Delta L/L_0)/T]$ versus time, t. Woolfrey *et al.* [15] suggested that the value m can be also determined by performing the experiments with different heating rates. They found that there was a relationship between relative shrinkage, $(\Delta L/L_0)_T$, and heating rates, C, as follows:

$$(\Delta L/L_0)_T = A_3 C^{-\frac{1}{m+1}} \quad (5)$$

The natural logarithmic form of Equation 5 should be:

$$\ln(\Delta L/L_0)_T = -\frac{LnC}{m+1} + \ln A_3 \quad (6)$$

Based on Equation 6, the straight line of slope $[-1/(m+1)]$ can be obtained from the plot of relative shrinkage at a specific temperature versus heating rates.

2.2. Model 2

Based on the work of Young and Culter [14], Wang and Raj [16] considered the effect of the density and grain size of samples on densification rate, and built up the following equation:

$$\dot{\rho} = A\frac{e^{-\frac{Q}{RT}}}{T}\frac{f(\rho)}{d^n} \quad (7)$$

and

$$A = \frac{k\gamma V^{2/3}}{R} \quad (8)$$

where $\dot{\rho} = d\rho/dt$ is the instantaneous rate of densification, d is the grain size, γ is the surface energy, V is the molar volume, R and T have the common meaning, Q is the activation energy, and $f(\rho)$ is a function of density. k is a constant and A is a material parameter that is insensitive to d, T or ρ. The grain size power law, n, has the value of $n = 3$ for lattice diffusion and $n = 4$ for grain boundary diffusion mechanism.

The experimental results can be dealt with by the following way:

$$\dot{\rho} = \frac{d\rho}{dt} = \frac{d\rho}{dT}\frac{dT}{dt}(dT \neq 0) \quad (9)$$

where $\frac{dT}{dt}$ means heating rate, C. The Equation 9 can be written:

$$\dot{\rho} = \frac{d\rho}{dT}C \quad (10)$$

Substituting Equation 10 into Equation 7 and taking logarithm we obtain:

$$\ln\left(\frac{d\rho}{dT}TC\right) = -\frac{Q}{RT} + \ln[f(\rho)] + \ln A - n\ln d \quad (11)$$

Due to the isotropic shrinkage of the samples during sintering processing, the density, ρ, can be expressed by the formula [16]:

$$\rho = (L_f)^3\rho_f\left[L_{(t)}\right]^{-3} \quad (12)$$

and

$$L_{(t)} = L_0 - \Delta L_t \quad (13)$$

where L_f is the final length of the sample, L_t is the time-dependent length equal to the value of $(L_0 - \Delta L_t)$ (L_0 is the original length of the sample and ΔL_t is the displacement of the sample at a certain time, t) and ρ_f is the final density obtained from the mass and dimension of the sample.

Inserting Equation 13 into Equation 12 gives:

$$\rho = (L_f)^3\rho_f(L_0 - \Delta L_t)^{-3} \quad (14)$$

Differentiating both sides of Equation 14 with respect to time:

$$\frac{d\rho}{dt} = 3(L_f)^3\rho_f(L_0 - \Delta L_t)^{-4}\frac{d\Delta L_t}{dt} \quad (15)$$

Both values of ΔL_t and $\frac{d\Delta L_t}{dt}$ can be obtained from the dilatometer. Therefore, it is easy to obtain the value in the left hand of Equation 11.

We have analysed our experimental results using the above two models. The findings are presented and discussed.

3. Experimental procedure

3.1. Sintering experiments

The characteristics of the raw powders, i.e., CeO_2 and Fe_2O_3, were reported elsewhere [10]. The samples with Fe/Ce atomic ratios ranging from 0 to 0.5% were prepared by the mixed-oxide technique. Sintering studies

were performed in a vertical dilatometer (Setsys 16/18, Setaram, France). The dilatometer allowed continuous monitoring of axial shrinkage. Two sets of sintering schedules were used, i.e., constant-heating-rate (CHR) sintering and isothermal sintering. During the CHR experiments, the samples were heated at a constant rate of 5, 10 and 20 K/min to a desired temperature and then cooled to room temperature. Isothermal sintering was conducted in the temperature range of 1000 to 1350°C. The samples were heated up to a desired temperature at a heating rate of 15 K/min and then held at this temperature for 1 to 3 h, after that the sample were cooled down to room temperature.

3.2. Measurement of grain size

Well-polished surface after thermal etching, was observed using scanning electron microscopy (SEM) (JSM-5410, Oxford, U.K.). Crystallite sizes were measured from SEM micrographs of the etched samples by the linear intercept technique described by Mendelson [17]. The average crystallite size, D, was obtained as follows: $D = 1.56\,L$, where L is the average grain-boundary intercept length of a series of random lines on the SEM photos.

4. Results

4.1. Model 1

Based on Equation 6, the plots of the natural logarithm of relative shrinkage at a particular temperature, $(\Delta L/L_0)_T$, against heating rate, C, can be obtained for different compositions (i.e., pure CeO_2, 0.25 and 0.5% Fe doped CeO_2). One of these plots is shown in Fig. 1 for pure CeO_2. The value, $(1/(m+1))$, and linear regression coefficient, R, at different temperatures are listed in Table I. The average values of m for pure CeO_2, 0.25 and 0.5% Fe doping are 0.97, 0.17 and -0.019, respectively.

Fig. 2 shows the plot of $\ln(t)$ versus $\ln(\Delta L/L_0)$ under isothermal sintering condition for pure CeO_2 and 0.5% Fe doping according to Equation 4. The values, m, obtained from the slopes for pure CeO_2 and 0.5% Fe doping are 0.677 and -0.22, respectively.

In order to calculate the apparent activation energy, three different heating rates, i.e., 5, 10 and 20 K/min,

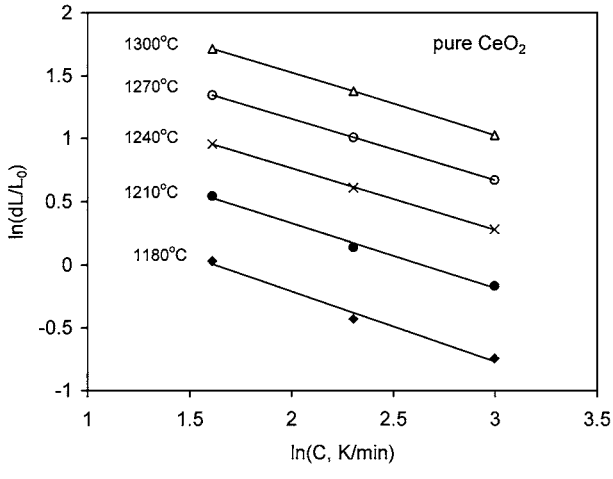

Figure 1 $\ln(\Delta L/L_0)_T$ versus $\ln(C)$ for pure CeO_2.

TABLE I The values of $1/(m+1)$ and linear regression coefficient, R, for different compositions

Temperature (°C)	1180	1210	1240	1270	1300
Pure CeO_2					
$1/(m+1)$	0.559	0.512	0.486	0.485	0.495
R	0.994	0.997	0.999	0.999	0.999
0.25% Fe doping					
$1/(m+1)$	0.96	0.87	0.82	0.81	0.81
R	0.98	0.97	0.97	0.98	0.98
0.5% Fe doping					
$1/(m+1)$	1.025	1.019	1.015		
R	0.997	0.997	0.999		

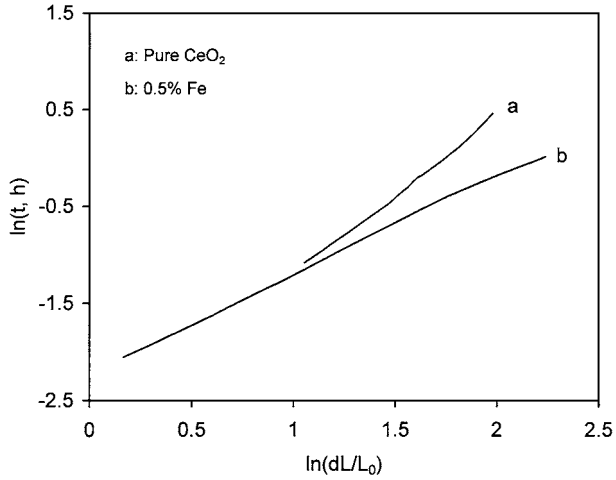

Figure 2 The relationship between natural logarithmic form of sintering time and relative shrinkage for (a) undoped and (b) 0.5% Fe-doped CeO_2.

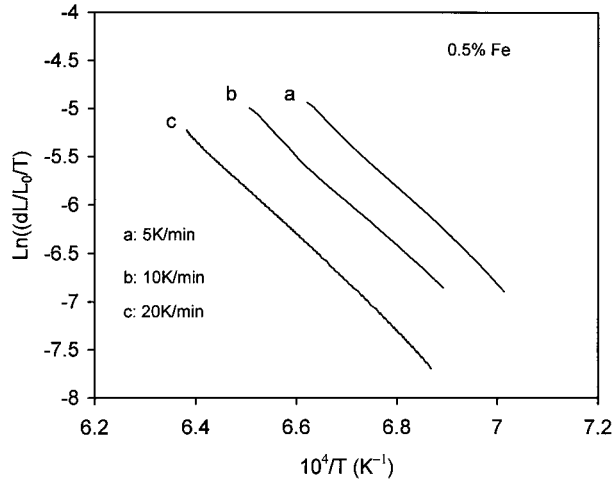

Figure 3 The natural logarithm of $(\Delta L/L_0)$ versus the inverse of temperature for 0.5% Fe-doped CeO_2 at heating rates of 5, 10 and 20 K/min, respectively.

were used for pure CeO_2, 0.25 and 0.5% Fe doping. The plots of $\ln[\Delta L/L_0)/T]$ versus $(1/T)$ of 0.5% Fe-doped CeO_2 is shown in Fig. 3 using Equation 3 in the relative shrinkage ranging from 1.5 to 8.5%. This shrinkage interval is just located in linear parts of curves at each heating rate, which reflects only one dominant sintering mechanism during the early sintering. It can be seen from this figure that three curves corresponding to three different heating rates exhibit almost the same slope. The average value of three slopes is used to calculate

TABLE II Power law, m, and activation energy, Q, for different compositions

	Based on Equation 6		Based on Equation 4	
Compositions	m	Q (KJ/mole)	m	Q (KJ/mole)
Pure CeO_2	0.97	365	0.677	311
0.25% Fe	0.17	395		
0.5% Fe	−0.019	396	−0.22	315

the apparent activation energy. The activation energy, Q, and exponent, m, of pure CeO_2, 0.25 and 0.5% Fe-doped CeO_2 are listed in Table II.

4.2. Model 2

Both values of ΔL_t and $\frac{d\Delta L_t}{dt}$ can be obtained from the dilatometer. Therefore, it is easy to obtain the value in the left hand of Equation 11. If one obtains the values of grain size (d) and densities, $f(\rho)$, the activation energy, Q, can be calculated for a known sintering mechanism. Alternatively, the activation energy can be determined by plotting $\ln(\frac{d\rho}{dT}CT)$ versus $1/T$ at constant values of ρ and d. In the present experiments, it was found that the grain size for pure CeO_2 and 0.5% Fe-doped sample does not change significantly below ~82% R.D. as shown in Fig. 4. A rapid grain growth occurs in the samples with relative density greater than 85%. Some investigators reported that grain growth in the intermediate stage of sintering could be suppressed by carefully preparing uniform packing in the green state; onset of grain growth was delayed until the state of the porosity changed from being open and interconnected to closed and isolated. Raj *et al.* [18] and Nadand *et al.* [19] reported that the grain size remained unchanged until relative density reached about 90%. For our case, however, the onset of grain growth occurs at ~85% R.D., which may be due to non-uniform grain size in the green state.

The derivatives of ρ with respect to temperature, T, for pure CeO_2 and 0.5% Fe doping are shown in Fig. 5a and b. For simplicity, the results at only two heating rates, 5 K/min and 10 K/min, are included.

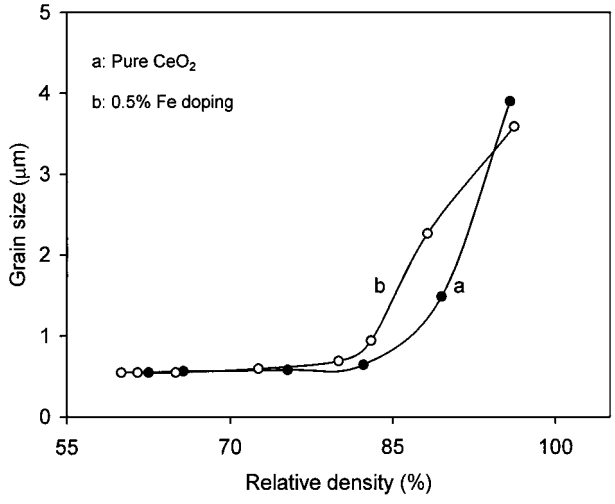

Figure 4 Grain size vs relative density for (a) pure CeO_2 and (b) 0.5% Fe doping.

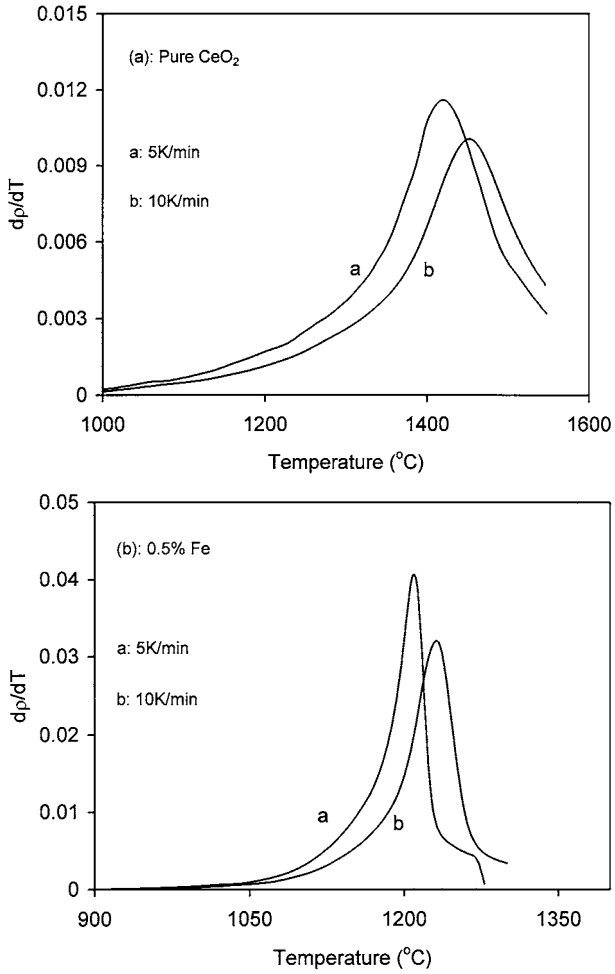

Figure 5 The derivatives of densities (ρ) with respect to temperature versus temperature for (a) pure CeO_2 and (b) 0.5% Fe doping.

Compared with the results of pure CeO_2 (Fig. 5a), Fe doping (Fig. 5b) obviously promotes the densification rate and reduces sintering temperatures.

In order to avoid the effect of grain growth, the density interval in the range of 60 to 80% R.D. is chosen for the calculation of activation energy. Fig. 6 a and b show Arrhenius plots derived from Equation 11, each curve corresponds to a given density, and each given density curve is drawn using three different heating rates, 5, 10 and 20 K/min. As shown in Fig. 6, these given density curves are almost parallel. It indicates that each curve has almost the same slope. The apparent activation energy for the sintering of pure CeO_2 and 0.5% Fe-doped CeO_2 are about 370 KJ/mole and 383 KJ/mole, respectively, which agrees well with the former values obtained from Equation 1. This result confirms that the information concerning sintering obtained from Model 1 is correct, although Model 1 doesn't concern about the effects of grain growth and density of samples. This is because the effects of grain growth and density is ignored in the relative shrinkage ranging from 1.5 to 8.5% which is used to fit the sintering kinetics in model 1.

5. Discussion

According to the classical model, i.e., Equation 6, we obtain the power laws m for pure CeO_2 and 0.5% Fe

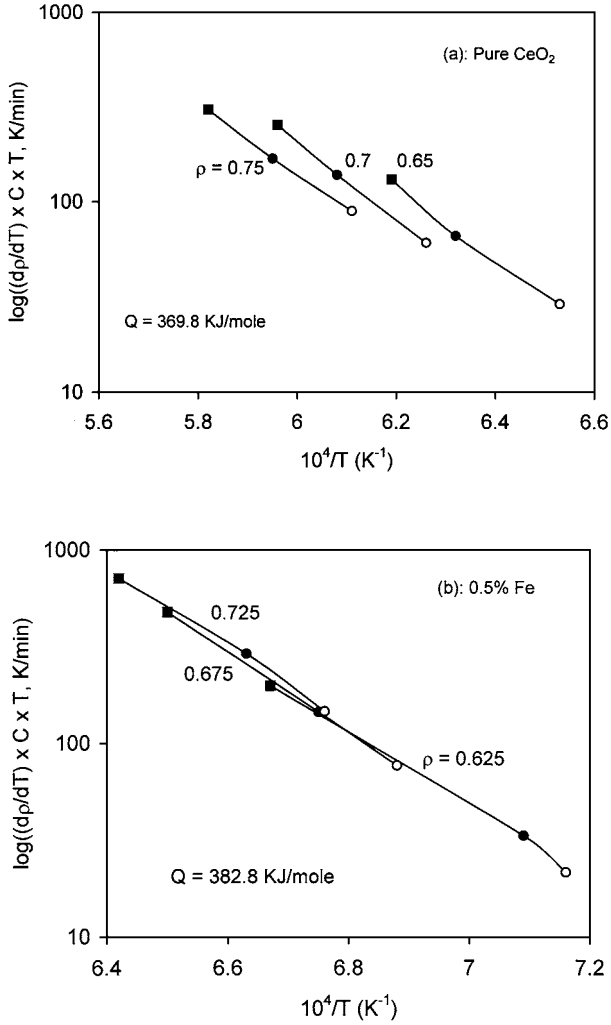

Figure 6 Arrhenius plots for the densification of (a) pure CeO_2 and (b) 0.5% Fe doping (o: 5 K/min, ●: 10 K/min and ■: 20 K/min).

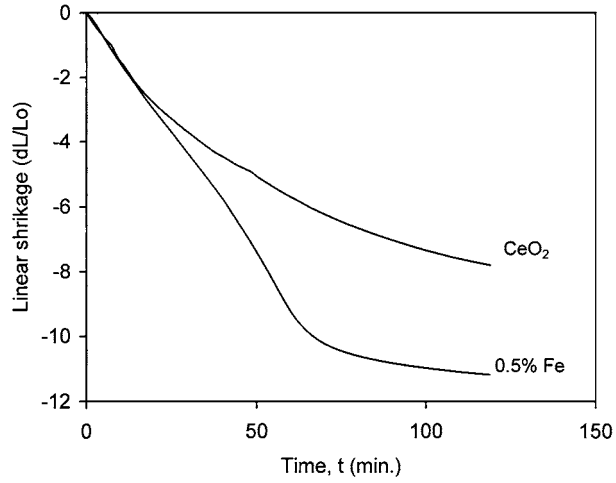

Figure 7 Linear shrinkage versus sintering time, t, for pure $CeO_2$and 0.5% Fe doping.

$$\frac{\Delta L}{L_0} = \frac{1}{3}\frac{\Delta V}{V_0} \propto t^{1+y} \tag{16}$$

where $\Delta V/V_0$ is the relative volume shrinkage, and exponent $y(\leq 1)$ depends on microstructure of a compact. The plot of $\Delta L/L_0$ versus t is shown in Fig. 7 for undoped and 0.5% Fe-doped CeO_2. It can be seen that a good linear part up to relative shrinkage of over 10% occurs for 0.5% Fe-doped CeO_2, while no linear parts can be found for pure CeO_2. This result is consistent with viscous flow mechanism that dominates the early-stage sintering for Fe-doped samples.

Although viscous flow mechanism usually occurs in a liquid phase sintering, Frenkel [21] proposed that under the influence of surface tension, crystalline powders could exhibit a viscous flow similar to that of amorphous powders. Bonnet *et al.* [22] found that small amount (∼1 mol%) of copper oxide resulted in an obvious shrinkage behavior of SnO_2 at low sintering temperature, 800 or 850°C, compared with pure SnO_2. In this range of temperature, it is impossible for the appearance of a liquid phase. However, they confirmed that the diffusion of copper ions on the surface of SnO_2 occurred at temperatures as low as 400°C, and the sintering kinetics of 1% Cu-doped SnO_2 could be fitted by the model proposed by Scherer to describe viscous flow sintering. Gouvea *et al.* [23] investigated the sintering behavior of MnO_2-doped SnO_2, and observed the segregation of MnO_2 on the surface of SnO_2 grains during sintering. Paria *et al.* [24] also examined the effect of MnO_2 doping on the sintering of SnO_2 and proposed a mechanism for mass transport based on viscous flow to explain the densification promoted by this dopant. From the periodical properties of elements, Fe element is the neighbor of the above-mentioned two elements (i.e., Mn and Cu). It is reasonable to assume, therefore, that Fe ions exhibit the same effect on the densification of CeO_2. Fe doping may change the surface tension of CeO_2 grains due to the diffusion of Fe ions onto CeO_2 grains during sintering. The local strain in some contact points of CeO_2 particles may be changed, which lead to the rearrangement of CeO_2 particles.

It can be observed, on the other hand, that the transition of sintering mechanisms from volume diffusion

doping are 0.97, and −0.019, respectively. It can be assumed that pure CeO_2 should be volume-diffusion controlled sintering (the ideal value of m equal to 1), while small negative value of m for 0.5% Fe doping exhibits viscous flow mechanism (the ideal value of $m = 0$). The power law m obtained from Equation 4 listed in Table II further confirms the viscous flow mechanism dominates the early-stage sintering of 0.5% Fe-doped CeO_2. It seems rather strange because this kind of sintering mechanism usually occurs in liquid-phase sintering, which can easily lead to grain boundary slide and rearrangement of particles in a compact. In the temperature range used (i.e., room temperature to 1500°C), Fe_2O_3 can not become a liquid phase because of its melting point of 1596°C. In addition, TG-DTA (thermal gravimetric and differential thermal analysis) measurement was conducted in air in the temperature ranging from room temperature to 1450°C for 5% Fe-doped CeO_2 and pure CeO_2, which give a very similar result for both samples. This result also indicates that no liquid phase is formed between Fe_2O_3 and CeO_2 below 1450°C.

Kingery *et al.* [20] proposed that if the densification was dominated by a viscous flow mechanism, there existed a linear relationship between relative shrinkage ($\Delta L/L_0$) and time (t), i.e.:

to viscous flow depends on Fe content, based on the results listed in Table I. Early-stage sintering of 0.25% Fe-doped CeO_2 may be cooperated by both mechanisms, although viscous flow mechanism is a dominate one during sintering. Unlike pure CeO_2 and 0.5% Fe-doped sample, 0.25% Fe doping has a poor linear regression coefficient, R, as listed in Table I, which conforms the former speculation, while a small value of power law, m, indicates that viscous flow mechanism play an important role in sintering.

On the other hand, the activation energy for viscous flow mechanism should be far smaller than that of volume diffusion mechanism. However, the activation energy for undoped and Fe-doped samples obtained from two different models (i.e., Equations 1 and 11) gives a very close value. It can be clarified using the formula suggested by Raj *et al.* [16]. They presented the following equation based on Equations 7 and 9:

$$\frac{Q}{R} = T_p^2 \left(\frac{\mathrm{d}\rho}{\mathrm{d}T}\right)_p \left[\frac{-f'(\rho)}{f(\rho)}\right]_p \tag{17}$$

where it is assumed that $Q \geq RT$ and $f'(\rho)$ is the derivative of $f(\rho)$ with respect to ρ. The quantity $\frac{\mathrm{d}\rho}{\mathrm{d}T}$ is obtained experimentally and is shown in Fig. 5a and b. Each curve of $\mathrm{d}\rho/\mathrm{d}T$ versus T exhibits a peak. The height of the peak and position are given by $(\frac{\mathrm{d}\rho}{\mathrm{d}T})_p$ and T_P, respectively. For a qualitative comparison, the effect of $[\frac{f'(\rho)}{f(\rho)}]_P$ can be ignored. Therefore, Equation 17 indicates that a higher peak temperature and greater height of the peak lead to a larger activation energy. Based on this equation, the comparison can be made according to the results as shown in Fig. 5a and b. For a given heating rate (for example, 10 K/min), the ratio of $\frac{(T_p)^2_{\mathrm{Fe}}}{(T_p)^2_{\mathrm{Ce}}}$ (here Fe for 0.5% Fe doping and Ce for pure CeO_2) is about 0.78, while the ratio of $\frac{[(\mathrm{d}\rho/\mathrm{d}T)_p]_{\mathrm{Fe}}}{[(\mathrm{d}\rho/\mathrm{d}T)_p]_{\mathrm{Ce}}}$ is about 3.2. Therefore, it is obvious to see that a large activation energy of Fe-doped CeO_2 results mainly from a rapid densification rate.

Based on Equation 3, $\ln[\Delta L/L_0)/T]$ versus $1/T$ at a heating rate of 10 K/min is plotted in Fig. 8 for undoped and 0.5% Fe-doped CeO_2. Unlike the results for the ZrO_2-Y_2O_3-CeO_2 system reported by Boutz *et al.* [25], three linear parts could be recognized, one at high and two at lower temperatures. They inferred that two linear parts in low temperature range indicated that there were two parallel-concurrent mechanisms that dominated the early-stage sintering. For our case, however, only two linear parts can be identified for both samples. The first linear part for pure CeO_2 occurs in the temperature range of 1255 to 1420°C, which corresponds to the relative shrinkage range of 1.1 to 7.1%, while the first one for 0.5% Fe doping occurs at 1185 to 1260°C, which corresponds to the relative shrinkage range of 1.1 to 10.2%. The relative density at 1420°C for pure CeO_2 and 1260°C for 0.5% Fe doping are about 78% and 87%, respectively. By referring to the results reported in [10], we can see these two relative densities just correspond to the appearance of maximum shrinkage rates for both samples. It suggests that volume diffusion and viscous flow are dominate densifying mechanisms for pure CeO_2 and Fe-doped samples, respectively.

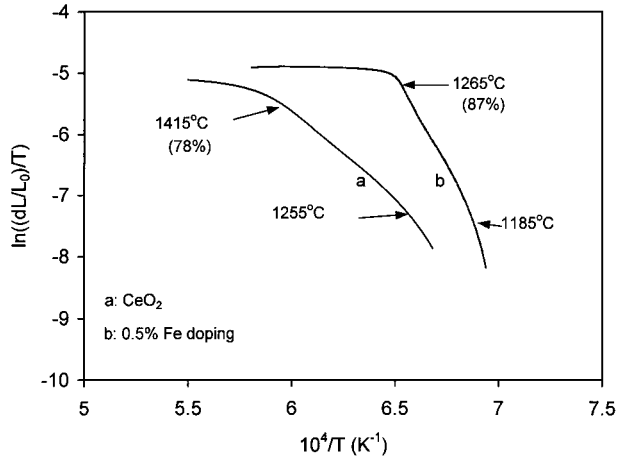

Figure 8 The natural logarithm of $[(\Delta L/L_0)/T]$ versus the inverse of temperature for pure CeO_2 and 0.5% Fe doping at a heating rate of 10 K/min (the values of relative density shown in the brackets).

It is interesting to note that some transition metal oxides (TMO), such as MnO_2, Fe_2O_3, CoO and CuO, have been proven to be effective sintering aids for the densification of some metal oxides (e.g., SnO_2, CeO_2, TiO_2 and Al_2O_3) [26–30]. Various explanations on the enhanced densification have been given including the liquid phase sintering. Based on our present study and previous work [22–24], however, a viscous flow mechanism has been identified to dominate the early-stage sintering of these metal oxides doped with a small amount of these TMOs. A viscous flow mechanism easily occurs in metal oxides (i.e., SnO_2, CeO_2, TiO_2 and Al_2O_3) doped with the above-mentioned TMOs due to the nature of these TMOs. These TMOs can easily diffuse on the surface of matrix particles at very low temperatures to form a thin amorphous film around particles as observed by many investigators [22, 24, 28, 29, 31]. It is well known that the extent of rearrangement of particles relies on the inter-particle friction. This thin amorphous film formed from these TMOs reduces the inter-particle friction, leading to the occurrence of a viscous flow mechanism.

6. Conclusions

The sintering kinetics of undoped and Fe-doped CeO_2 has been fitted, based on two sintering models. It is identified that pure CeO_2 should exhibit a volume-diffusion controlled sintering, while the sintering of Fe-doped samples is dominated by viscous flow mechanism. The transition of sintering mechanisms from volume diffusion to viscous flow depends on the Fe content. Viscous flow mechanism dominates the early-stage sintering of 0.5% Fe-doped sample. It seems that below 0.5% Fe doping level, the early stage sintering may be cooperated by both mechanisms (i.e., volume diffusion and viscous flow). For 0.5% Fe-doped sample, a viscous flow dominates the sintering until the relative density reaches ~87%.

Based on our present and previous work, It is believed that a viscous flow mechanism dominates the

early-stage sintering of some metal oxides (i.e., SnO_2, CeO_2, TiO_2 and Al_2O_3) doped with a small amount of some TMOs. This is due to the nature of these TMOs, which can easily diffuse on the surface of matrix particles at very low temperatures to form a thin amorphous film around particles. This thin amorphous film reduces the interparticle friction, leading to the occurrence of a viscous flow mechanism.

References

1. K. EGUCHI, T. HATAGISHI and H. ARAI, *Solid State Ionics* **86–88** (1996) 1245.
2. J. F. BANMARD, P. PAPET and P. ABELARD, *Sci. Tech. Zircionia III* **24B** (1986) 779.
3. J. DRENNAN and S. P. S. BADWAL, *ibid.* **24B** (1986) 855.
4. H. INABA and H. TAGAWA, *Solid State Ionics* **83** (1996) 1.
5. J. VAN HERLE, T. HORITA, T. KAWADA, N. SAKAI, H. YOKAKAWA and M. DOKIYA, *ibid.* **86–88** (1996) 1255.
6. K. ZHENG, B. C. H. STEELE, M. SAHIBZADA and I. S. METCAFE, *ibid.* **86–88** (1996) 1241.
7. M. A. PANHANS and R. N. BLUMENTHAL, *ibid.* **60** (1993) 279.
8. Y. S. ZHEN, S. J. MILNE and R. J. BROOK, *Sci. Ceram.* **14** (1988) 1025.
9. Y. C. ZHOU and M. N. RAHAMAN, *J. Mater. Res.* **8** (1993) 1680.
10. ZHANG TIANSHU, PETER HING, HAITAO HUANG and J. KILNER, *J. Mater. Proc. Tech.* **113** (2001) 463.
11. R. L. COBLE, *J. Appl. Phys.* **32** (1961) 787.
12. Z.-Z. DU and A. C. F. COCKS, *Int. J. Solid Struct.* **31** (1994) 1429.
13. M. J. BANNISTER, *J. Amer. Ceram. Soc.* **51** (1968) 548.
14. W. S. YOUNG and I. B. CUTLER, *ibid.* **53** (1970) 659.
15. J. L. WOOLFREY and M. J. BANNISTER, *ibid.* **55** (1972) 390.
16. J. WANG and R. RAJ, *ibid.* **73** (1990) 1172.
17. M. I. MENDELSON, *ibid.* **52** (1969) 443.
18. C. P. CAMERON and R. RAJ, *ibid.* **71** (1988) 1031.
19. N. NADAUD, D. KIM and P. BOCH, *ibid.* **80** (1997) 1208.
20. W. D. KINGERY, *J. Appl. Phys.* **30** (1959) 301.
21. J. FRENKEL, *J. Phys.* **9** (1945) 385.
22. J. P. BONNET, N. DOLET and J. M. HEINTZ, *J. Eur. Ceram. Soc.* **16** (1996) 1163.
23. D. GOUVEA, J. A. VARELA, A. SMITH and J. P. BONNET, *Eur. J. Soli Statr Inorg. Chem.* **33** (1996) 345.
24. M. K. PARIA, S. BASU and A. PAUL, *Trans. Indian Ceram. Soc.* **42** (1983) 90.
25. M. M. R. BOATZ, A. J. A. WINNUBST and A. J. BURGGRAAF, *J. Europ. Ceram. Soc.* **13** (1994) 89.
26. J. P. BONNET, N. DOLET and J. M. HEINTZ, *ibid.* **16** (1996) 1163.
27. J. ACERRI, E. R. LEITE, D. GOUVEA, E. LONGO and J. A. VARELA, *J. Amer. Ceram. Soc.* **79** (1996) 799.
28. D.-W. KIM, T.-G. KIM and K. S. HONG, *Mater. Res. Bulletin* **34** (1999) 771.
29. C. KLEINLOGEL and L. J. GAUCKER, *Solid State Ionics* **135** (2000) 567.
30. S. SUMITA and H. KENTBOWEN, in "Ceramic Transactions: Ceramic Powder Science II, *B*, edited by Gary L. Messing, Edwin R. Fuller, Jr. and Hans Hausner, (1987) p. 840.
31. G. S. LEWIS, A. ATKINSON and B. C. H. STEELE, in *Proc. 4th Europ SOFC Forum*, edited by A. McEvoy (2000) Vol. 2, p. 773.

Received 24 October 2000
and accepted 16 October 2001